Version of Record: https://www.sciencedirect.com/science/article/pii/S0025540818301697
Manuscript_acdd4de44b2f5aa4c0d8e6625bec09e8

Alkoxysilane effect in hybrid material : A comparison of pHEMA-TiO_2 and pMAPTMS-TiO_2 nanoparticulate hybrids

P. Gorbovyi,[1] A. P. Diaz-Gomez[1], M. Traore,[1#] L. Museur,[2] L. Rozes,[3] F. Ribot,[3] C. Sanchez,[3] A. I. Kuznetsov,[4*] B. N. Chichkov,[4,5] A. Kanaev [1]

[1] *Laboratoire des Sciences des Procédés et des Matériaux, CNRS, Université Paris 13, Sorbonne Paris Cité, 93430 Villetaneuse, France*

[2] *Laboratoire de Physique des Lasers - LPL CNRS, Université Paris 13, Sorbonne Paris Cité, 93430 Villetaneuse, France*

[3] *Sorbonne Universités, UPMC Univ Paris 06, CNRS, Collège de France, UMR 7574, Chimie de la Matière Condensée de Paris, F-75005, Paris, France.*

[4] *Laser Zentrum Hannover e.V., Hollerithallee 8, 30419 Hannover, Germany*

[5] *Federal Scientific Research Centre "Crystallography and Photonics" RAN, Leninskiy prospekt 59, Moscow 119333, Russia*

[#] corresponding author. E-mail: traore@lspm.cnrs.fr
[*] present address : Data Storage Institute, Advanced Concepts and Nanotechnology Division, Singapore

Abstract

We report on a comparative study of photonic sensitivities of organic-inorganic hybrids prepared with size-selected 5nm titanium-oxo-alkoxo nanoparticles and two different organic phases: HEMA (2-hydroxyethyl methacrylate) and MAPTMS (3-methacryloxypropyltrimethoxysilane). After organic polymerization, the obtained pHEMA-TiO_2 and pMAPTMS-TiO_2 hybrids are solids with different inter-component bindings. While surface exchange fixes organic (HEMA than pHEMA) groups on the nanoparticle surface, the titanium-oxo-alkoxo nanoparticles do not interact with the organic component in the pMAPTMS-TiO_2 hydrid. Indeed, MAPTMS molecules are hydrolyzed forming condensed Si-O-Si species. The formation of Si-O-Ti bonds is observed at the organic thermal polymerization stage, which may be a signature of the silica layer formation at the particles surface. Consequently, the quantum efficiency of the photoinduced charge separation and storage in pMAPTMS-TiO_2 hybrids is found considerably lower compared to that in pHEMA-TiO_2 hybrids. The 3D micro-structuring of the hybrid solutions has been realized using 2-photon laser polymerization. The structures were mechanically more stable and easier to achieve in pMAPTMS-TiO_2 compared to pHEMA-TiO_2. Moreover, higher density of the photoinduced electrons decreases the damage threshold in the pHEMA-TiO_2 hybrids.

Keywords: A. Hybrids, A. nanostructures, B. Sol-gel chemistry, B. Optical properties.

1. Introduction

For over two decades, methods of preparing inorganic and hybrid nanomaterials based on "soft chemistry" have attracted strong interest both in academia and industry[1-4]. Hybrid materials advantageously mix structural flexibility and convenient processing of polymer with electronic properties of inorganic component. Consequently, they are promising candidates for potential application in many fields, such as electronics, optics, biology, etc.

Considerable progress has been reached in elaboration of organic-inorganic hybrids and understanding of their physical properties. Between them, silica, titania, and zirconia hybrids attract particular interest for applications in 2-photon laser microstructuring due to their high refractive index and biocompatibility[5-8]. Furthermore, titania hybrids show interesting electron transport properties, consisting in the effective photoinduced charge separation across the large internal organic-inorganic interface[9-11], which permits laser writing of 3D domains with modified physical properties[12]. More recently, it has been established that the modification of the refraction index of irradiated domains can attain $\Delta n=-0.005$[13], which may enable fabrication of optical waveguides in these materials. Titania hybrids, capable accumulating of up to 10 % Ti^{3+} centers, were proposed for photochemical conversion and solar energy storage[14-15].

A capacity of the titania solids to effectively separate and store charges has attracted much attention in the past[16-18]. This ability is related to the presence of photo-excited hole scavengers and positive electron affinity of Ti^{4+} centers. It has been recognized that an adequate design of the material nanoscale interface can considerably increase the efficiency of charge separation and storage process. While the typical efficiency in the range of 1-10 % has been reported in early studies, late developments of the hybrids have promoted the process efficiency up to 50%[19] and even higher values[20-21].

In consequence, the elaboration process is crucial for electronic properties of the hybrid materials. A control of the inorganic-organic interface and nanoscale morphology, including the inorganic particle sizes and aggregation state, permits to promote the photoinduced charge separation efficiency of these materials and increase their photonic sensitivity. Despite of the key functional role of the inorganic titania component, much attention has to be paid to the organic component, since recombination of photogenerated charges depend on their capacity to trap the photoexcited hole. It is therefore of high interest to compare photonic sensitivities of the materials prepared with different organics, which can or cannot produce strong interaction with the inorganic component.

In this paper, we report on the effect of alcoxysilane as a molecular precursor of the polymer matrix embedding TiO_2 nanoparticles. A comparative study was carried out of organic-inorganic hybrid materials prepared of size-selective non-aggregated 5nm TiO_2 nanoparticles with two different organic phases: 2-hydroxyethyl methacrylate (HEMA) and methacryloxypropyltrimethoxysilane (MAPTMS).

2. Experiment and sample preparation

2.1 Material preparation

The preparation schema adopted for pHEMA-TiO_2 and pMAPTMS-TiO_2 hybrids was previously described by Gorbovyi et al.[19]. In short, the size-selected 5 nm titanium-oxo-alkoxo (TOA) nanoparticles were generated in a thermostatic sol-gel reactor with rapid micromixing[22-23], using titanium tetraisopropoxyde (TTIP) precursor (Acros Organics, 98% purity) and distilled water in 2-propanol (Acros Organics, 99.5% purity) solution and the hydrolysis ratio H=2.0 at 20.0 °C. The underlying sol-gel chemistry does not proceed via hydroxide intermediates, but

results directly in well-defined titanium-oxo-alkoxo species through one-step hydrolysis-condensation transformation associated with profound restructuring of the precursor molecules[24]. In our experimental conditions, the protected from external humidity nanocolloids are almost monodispersed and stable beyond one day[25], which allows their relatively simple manipulations.

At the second step, the solvent exchange (2-propanol by HEMA or MAPTMS) was carried out overnight in vacuum. The both monomers were preliminary distilled in order to eliminate impurities and inhibitors of spontaneous polymerization. The procedure is performed in a round-bottom flask, equipped with magnetic stirrer and vacuum valve. A single stage membrane pump (KNF N 840.3FT.18) was used for pressure reduction down to 10 mbar. A LN2 trap was used to condensate the 2-propanol vapors. The exchange reactor temperature control was performed with a simple water bath (20 °C). The adjustment of the inorganic nanoparticle concentration was performed at this stage. By this method, the hybrid solutions with Ti concentrations from 0.15 mol/l (x1) to 3.0 mol/l (x20) have been prepared (Table 1).

The nanoparticulate precursors were stable in dry atmosphere, e.g. x1 sample could be conserved over 1 month.

At the final step, free radical polymerization of the methacrylate functions was produced thermally or photochemically from the prepared monomer-TiO_2 solution. The thermal polymerization was conducted at 90 °C during 12 hours with an addition of the AIBN initiator. Photopolymerisation was conducted with an addition of the Igacure-369 photoinitiator using two types of lasers: UV picosecond (355 nm, ~10^{-11} s) and near-IR femtosecond (1030 nm, ~10^{-13} s) lasers. Two different mechanisms of initiation were involved: while UV irradiation triggers one-photon polymerisation process, the near-IR femtosecond laser pulses induce two-photon polymerization.

Table 1: Hybrid samples compositions. The last column shows relative volume increase of monomer solutions after the solvent exchange stage (impregnation of TOA nanoparticles).

Sample	TiO_2 colloid volume, ml	HEMA : Ti molar ratio	MAPTMS : Ti molar ratio	C_{Ti}, mol/l (hybrids)	ΔV/V HEMA / MAPTMS
x1	5	54.8:1	28.2 :1	0.15	0 / 0
x2	10	27.3 :1	13.9 :1	0.30	0 / 0
x5	25	11 :1	5.65 :1	0.75	0 / 0
x10	50	5.5 :1	2.82 :1	1.50	0 / 0.04
x15	75	3.7 :1	1.88 :1	2.25	0 / 0.08
x20	100	2.7 :1	1.41 :1	3.00	0 / 0.11

2.2 Material characterization

The particle size (2R) and the scattered light intensity (I) were measured at the nucleation and solvent exchange stage in situ with a monomode optical fiber probe of He-Ne laser by photon-correlated spectroscopy method, using 16-bit 255-channels digital correlator (*PhotoCor Instruments*). The observation volume defined by a mutual positioning of two monomode optical fibres is small enough (~10^{-6} cm^3) to prohibit multiple scattering events. The measurements (I,R) were carried out in the automatic sampling mode with the data accumulation over 60 s, which permits to reduce noisy data due to rare dust particles.

The ligands exchange during solvent exchange and C=C bonds opening during polymerization stages were monitored by Raman spectroscopy. The Raman spectra were measured with high-resolution micro-Raman spectrometer (HR800 HORIBA Jobin Yvon) operating at 633 nm wavelength with spectral and spatial resolution of 0.25 cm^{-1} and ~5 μm,

respectively. The scattered light was collected in a backscattering configuration and recorded on a Peltier-cooled CCD camera.

The NMR ^{17}O, ^{29}Si spectra in liquid and solid forms have been performed using Bruker Avance III 300 (300.13 MHz) spectrometer equipped with fiber BBFO 5mm. No additional deuterated solvents were used for sample preparation. Liquid (before organic polymerization) and solid (polymerized) hybrid samples were characterized with ^{17}O NMR method. The spectra acquisitions were performed at the following conditions: spin-echo (D1-90°-τ-180°-τ-AQ), where period of 90° pulse was 15.2 µs; delay echo was 100 µs, interpulse delay was 0.1 s and acquisition time was 4.1 ms (TD=4 K, SW=12300 ppm or 50000 Hz). 28800 scans were accumulated (~50min / exp). MAPTMS-TiO_2 samples were additionally characterized with the RMN ^{29}Si (59.62 MHz) method. The time proton "inverse gated" decoupling was performed. Impulse angle was 30° (~3 µs), acquisition time was 0.69 s (TD=16 K, SW=200 ppm ou 12000 Hz) and recycling time was 5 s. 1024 scans were accumulated (t~100 min) per acquisition.

Measurements of the photonic sensibility of prepared hybrids were carried out in pump-probe experiments. The pump, third-harmonics (λ=355 nm) of Nd:YAG laser (*Ekspla*), delivered 25-ps pulses at the repetition rate of 10 Hz. The UV-laser beam with the diameter of 5 mm interacts with the sample at normal incidence, and both incident and transmitted beams are analysed by two µJ-sensitive calorimeters C1 and C2 (*Coherent*). The UV-laser fluence <10 mJ/cm^2 was used to avoid any irreversible material damage. The probe cw-laser fiber coupled diode beam at 640 nm wavelength (*Thorlabs*) monitored the photoinduced absorption of the hybrid samples in the central part (D=1 mm) of the pump UV-laser interaction zone. The knowledge of the absorption cross-section at 640 nm $\sigma=1.3\cdot10^{-18}$ cm^2 [26] enables direct

quantitative measurements of the concentration of trapped electrons. The data acquisition is controlled using LabView software.

Laser-induced two-photon polymerization (2PP) has been carried out using second harmonic of Yb:glass femtosecond laser oscillator (λ=515 nm) delivering pulses of 150 fs duration with the repetition rate of 10 MHz. 2PP is a direct laser writing technique, which allows fabrication of complex computer-controlled 3D structures with a resolution below 100 nm[27-28]. It is based on laser initiation of polymerization reactions inside transparent photocurable materials. Due to nonlinear nature of the laser-material interaction, the polymerization process can be strongly localized in the focal point of the laser beam, which produces small polymerized voxels inside the non-polymerized material. Scanning the laser beam focus allows fabrication of arbitrary form computer-controlled polymerized structures. After removing of the non-polymerized part of the material, free-standing or attached to a substrate polymerized microstructures can be obtained. Big box-like structures were polymerized with the laser beam loosely focused by a 120 mm lens inside a thick flat layer of the hybrid material. These relatively large structures were produced in order to check photochromic response of the polymerized hybrids. In order to verify the ability of two-photon polymerization to reach submicronic spatial resolution, woodpile-like structures were fabricated with the tightly focused laser beam by 100X oil immersed microscope objective (Zeiss, Plan Apochromat, NA=1.4).

3. Results and Discussion

3.1 Structure and composition

The intensity auto-correlation function (ACF) contains information about the diffusion coefficient and hydrodynamic radius of the inorganic nanoparticles in monomer solutions.

The measured ACF is expresses by

$$g^{(2)}(\tau) = \frac{G^{(2)}(\tau)}{G^{(2)}(0)} = \frac{I_S(t).I_S(t+\tau)}{I_S^2(t)} = 1 + e^{-2Dq^2\tau} \quad (1)$$

where $q = \frac{4\pi n}{\lambda}\sin(\theta/2)$-is the scattering wave vector at the observation angle θ and light wavelength λ, D is the particle diffusion coefficient and τ is the correlation time. Since $D = \frac{kT}{6\pi nR}$ (η, n and T are respectively the dynamic–viscosity, refraction index and temperature of colloid and k is the Boltzmann constant), The exponential factor in Equation 1 can be presented as: $f(T, \theta, \lambda)R^{-1}\frac{n^2\tau}{\eta}$, where *f(T,θ,λ)* is the constant related to the experimental geometry and temperature. Tracing the experimental points in frame (g^2,-$\frac{n^2\tau}{\eta}$) permits easier comparison of the particles radii.

We used the refraction index / dynamic viscosity of HEMA and MAPTMS solutions (20°C), respectively 1.45 / 0.0059 Pa·s and 1.43 / 0.00260 Pa·s. The ACF curves of freshly prepared HEMA-TiO_2 and MAPTMS-TiO_2 solutions are shown in Figure 1 (a) and (b).

The decay of curve (b) is clearly longer compared to (a), which evidences larger TOA nanoparticles in the MAPTMS solution. The fit of the experimental curves following mono-exponential decay with Eq. (1) results in the mean particles radii 2.5 and 3.8 nm in HEMA and MAPTMS solutions, respectively, after the exchange stage. The larger size of the TOA nanoparticles in MAPTMS solution may be a trace of their agglomeration. Since the agglomeration state is a sensitive function of the nanoparticle number density in the solution, their size is expected to increase with the titania precursor concentration (C_{Ti}).

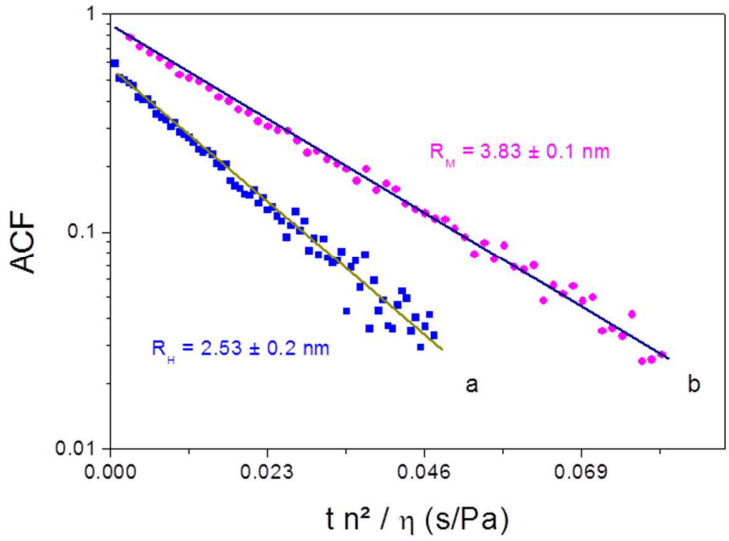

Figure 1. Characteristic ACF of oxo-TiO_2 nanoparticles after solvent exchange in the x10 solution with HEMA (a) and in x5 solution with MAPTMS (b).

The dependence of radius of HEMA and MAPTMS modified TOA nanoparticles on C_{Ti} is shown in Figure 2.

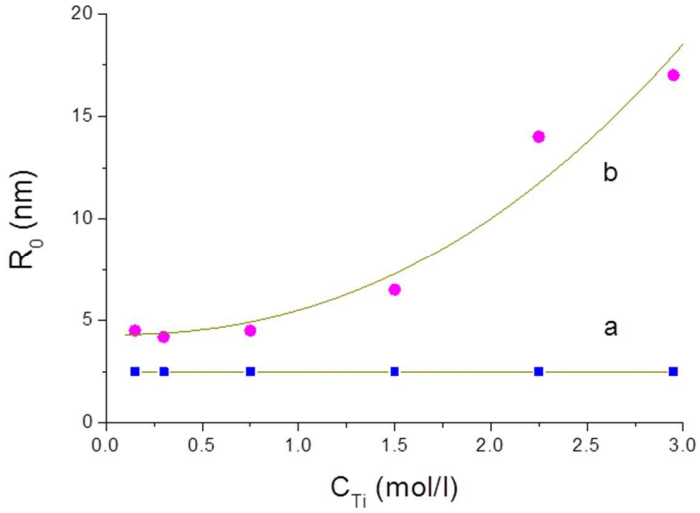

Figure 2. Initial radius R_0 of oxo-TiO_2 nanoparticles after 2-propanol solvent exchange with HEMA (a) and MAPTMS (b) versus titania concentration C_{Ti}.

As expected, the TOA nanoparticles conserve their initial size 2R=5 nm in HEMA solutions after the solvent exchange. On the other hand, their size in MAPTMS solution increases with C_{Ti}; however, this size dependence is strongly non-linear, and in the range of small concentrations $C_{Ti} \leq 0.75$ mol/l the size is almost constant. We therefore argue that this diameter of ~7.5 nm is inherent to TOA nanoparticles in MAPTMS environment and is not related to the agglomeration state. One possible explanation of the observed size increase consists in condensation of MAPTMS molecules around TOA nanoparticles. This hypothesis is supported by different affinities to water of these organic (hydrophobic) and inorganic (hydrophilic) components, which may result in trapping of water molecules in the TOA nanoparticle shell, which can promote MAPTMS hydrolysis. A presence of the residual water in hybrid solutions based on MAPTMS monomer can be supported by the total volume increase after the solvent exchange stage, documented in Table 1 (last column). Indeed, unlike HEMA solutions, volumes of freshly prepared MAPTMS hybrid solutions x10, x15 and x20 are larger than that of the added monomer. The precision of measurements and small losses of monomers under vacuum pumping make difficult confirmation of the volume increase in the samples with lower Ti concentration x1, x2, and x5.

More insights into the polycondensation of species in the hybrid MAPTMS-TiO_2 solutions were obtained from the NMR O^{17} experiments. A very low ^{17}O isotope natural abundance (0.039%) required its addition to the reaction medium. Therefore, we have used ^{17}O labeled 20.9% enriched water from Sigma Aldrich for the stage of TOA nanoparticles nucleation. The sol-gel process naturally produces hydrolysis-condensation reactions of the material enriched by ^{17}O. After solvent exchange stage, ^{17}O atoms take part of the oxo-core at the surface of TOA nanoparticles and, possibly, in residual traces of water in the colloidal solution. The condensation

of both Si-O-Si and Si-O-Ti bonds is expected to involve these ^{17}O atoms. We assume a similar reactivity of water molecules containing ^{16}O, ^{17}O, and ^{18}O isotopes.

The ^{17}O-NMR spectra of HEMA and MAPTMS based hybrid sample x10 are shown in Figure 3 (a) and (c) for liquid solutions and (b) and (d) for polymerized solids.

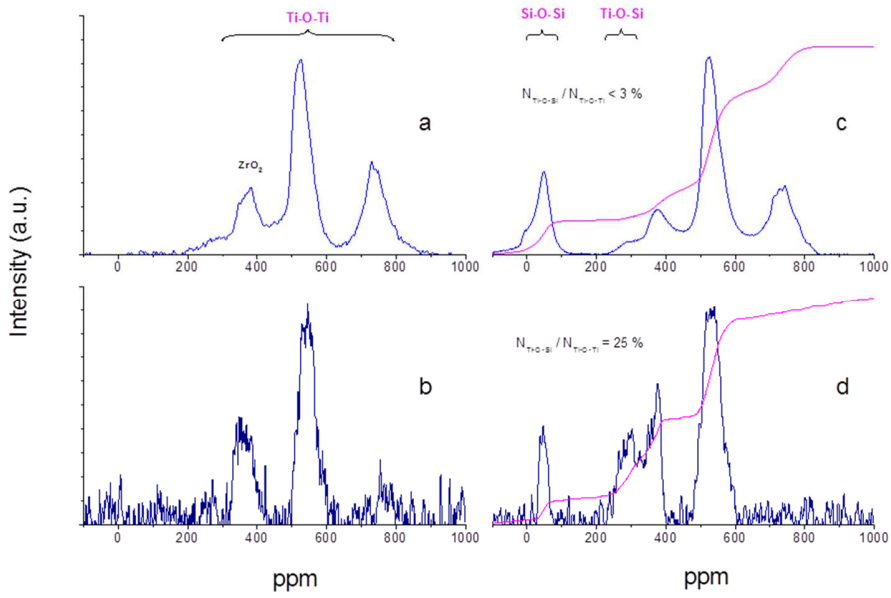

Figure 3. ^{17}O-NMR spectra of liquid HEMA-TiO_2 (a), solid pHEMA-TiO_2 (b), liquid MAPTMS-TiO_2 (c) and solid pMAPTMS-TiO_2 (d) hybrids, obtained after thermal organic polymerisation. The band at 370 ppm is due to ZrO_2 oxygen from the rotor, which contained analyzed samples.

Several bands are observed. The two main bands in HEMA and MAPTMS hybrids situated at 530 and 750 ppm (Figure 3a and 3c) are characteristic of Ti-O-Ti condensed species in OTi_4 and (OTi_3-OTi_2) coordinations. There is an intensification of the OTi_4 coordination in solid samples (Figure 3b and 3d), which can be related to a temperature increase[29] during the polymerization process. Two other bands situated at -30 and 70 ppm and characteristic of Si-OH

and Si-O-Si condensed species, were observed in MAPTMS hybrids spectra. In addition, the broad signal in the 200-300 ppm range can be assigned to Si-O-Ti bridges[30]. Complementary, liquid-state ^{29}Si NMR measurements of the MAPTMS-TiO_2 hybrids presented in Figure 4 support this conclusion.

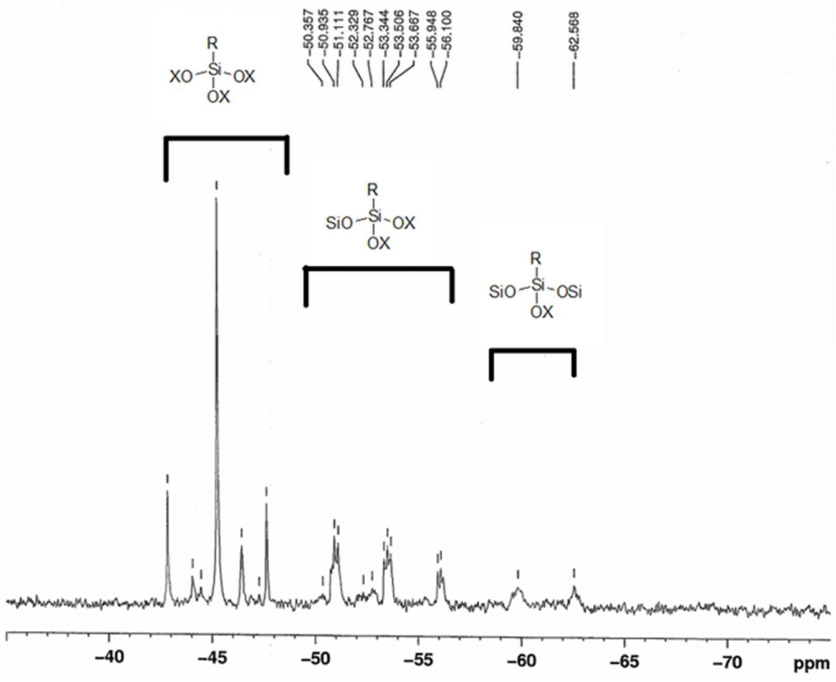

Figure 4. ^{29}Si NMR spectrum of MAPTMS-TiO_2 hybrids solutions, which confirms the formation of Si-O-Si bonds in liquid phase.

T0 peaks assigned to uncondensed precursor molecules can be clearly distinguished from -43 to -48 ppm, but T1 signals (from -50 to -56 ppm) and T2 peak (from -59 to -63 ppm) which correspond to Si atoms at the end of a chain and to species linked to two Si bearing an unreacted –OX function (X=H or CH_3). No T3 species are distinguishable due to a low reactivity of the precursor. Different contributions related to hydrolyzed and condensed products confirm the formation of two- and three-member inorganic polycondensated Si-O-Si chains in MAPTMS solvent. Although both oxygen contributions cannot be resolved at this stage, the integration of spectral area applied to MAPTMS-TiO_2 hybrid solutions indicates a relatively small number

density of possible Ti-O-Si bonds in comparison to Ti-O-Ti condensed bonds: $N_{Ti-O-Si} / N_{Ti-O-Ti}$ ≤3 % (figure 3c). A strong preference in formation of Si-O-Si bonds in comparison to Si-O-Ti bonds in liquid MAPTMS solutions suggests that hydrolysis-condensation reactions of silica species do not take place on the surface of TOA nanoparticles. In hydrophobic media, like MAPTMS monomers, free residual water can be confined in the surface layer of TOA nanoparticles which can catalyze their hydrolysis. This will promote hydrolysis-condensation of silica species preventing the contact with Ti-OH surface hydroxyls. Such spatial separation of the reaction regions involving Si and Ti atoms can explain the observed disproportion in the formation of Si-O-Si and Si-O-Ti bonds.

An inspection of this region in the solid phase has led us to a conclusion about more important contribution of the condensation reactions leading to the formation of Ti-O-Si bonds. This can be seen in the solid-state ^{17}O NMR spectrum of pMAPTMS hybrids presented in Figure 3 (d). After thermal polymerization, the intensity of Si-O-Si bonds (60-70 ppm region) is not significantly affected. On the other hand, the relative intensity of Ti-O-Si bonds considerably increases, up to 25 % with the concomitant disappearance of the Si-OH signal, and at the same time, the disappearance of (OTi_3-OTi_2) peaks characteristic to surface site. We can deduce that TOA nanoparticles promote MAPTMS hydrolysis reaction and NMR measurements prove the formation of a silica shell around the TiO_2 nanoparticles which leads to an increase in the size of nanoparticles.

Several studies have been realized on functionalization of TiO_2 nanoparticles with MAPTMS. Junlabhut et al.[31] have elaborated optical sensitive thin films by Ag nanoparticles doped SiO_2/TiO_2 hybrid deposition via sol-gel spin coating technique, Sedghi et al.[32] have synthesized hybrids by modifying the surface of the TiO_2 nanoparticles with MAPTMS and Ali[33] has

summarized synthesis methods and characterization techniques of sol-gel hybrid coatings. The formation of organic-inorganic interface has not been clearly addressed in these studies. Our particular preparation of the nanoparticulate hybrids may explain the formation of silica shell.

The integration of the TOA nanoparticles in HEMA has been previously studied[9,19]. These HEMA-TiO_2 hybrids were classified according to Sanchez[34] as belonging to Class II materials related by strong ion-covalent bonds between the organic and inorganic moieties.

In contrast to HEMA where ~40 % of Ti atoms receive OEMA ligands, the organic part of MAPTMS are not grafted on the TOA nanoparticles surface during the solvent exchange stage. We can conclude that conditions are created for the inorganic nanoparticles isolation from the polymer network. On the other hand, solid-state ^{17}O NMR spectrum of the polymerized hybrids presented in Figure 3d proves the formation of Si-O-Ti bonds, which relative number density increases by about 10 times. Consequently, the condensation process is induced by heating. At the same time, the fact that relative number of Si-O-Si bonds does not change during polymerization signifies that new hydrolyzed Si-OH species do not appear. The origin of these Si-O-Ti bonds may be explained by the formation of silica layer at the particle surface.

An additional comparison between HEMA-TiO_2 and MAPTMS-TiO_2 hybrids can be made by Raman spectroscopy. This method is based on observation of intensities of the characteristic peaks of C=C at 1407 and 1641 cm^{-1}, associated with $C=CH_2$ stretching and C=C aliphatic stretching vibrations of the organic monomers[19,34]. The thermal polymerization of the hybrid samples was carried out at 90°C until the process saturation attained after 24 hours. It was observed that additional polymerization at 120 °C during 3 hours does not improve the monomer-polymer conversion rate but induces yellow coloration of samples.

The residual fraction of the C=C double bonds in HEMA-TiO_2 and MAPTMS-TiO_2 solid samples is shown in Figure 5 as a function of Ti concentration (C_{Ti}). We observe that an addition

of the inorganic component does not affect the polymerization (almost 100 %) at relatively low concentrations $C_{Ti} \leq 0.75$ mol/l and considerably decreases the polymerization extent at higher Ti concentrations. Polymerization of the concentrated hybrid solutions does not result in complete C=C bonds opening. This has been earlier attributed to steric limitations in this nanoparticulate system[9,19]. Longer thermal polymerization (above 12 hours) and at higher temperatures (120 °C) only moderately (~5%) improves the polymerization extent. One can however see that the residual non-polymerized component is stronger in HEMA-TiO_2 (50%) compared to MAPTMS-TiO_2 (30%) hybrids, while in pure polymeric samples 100% double bonds conversion has been observed at the same conditions.

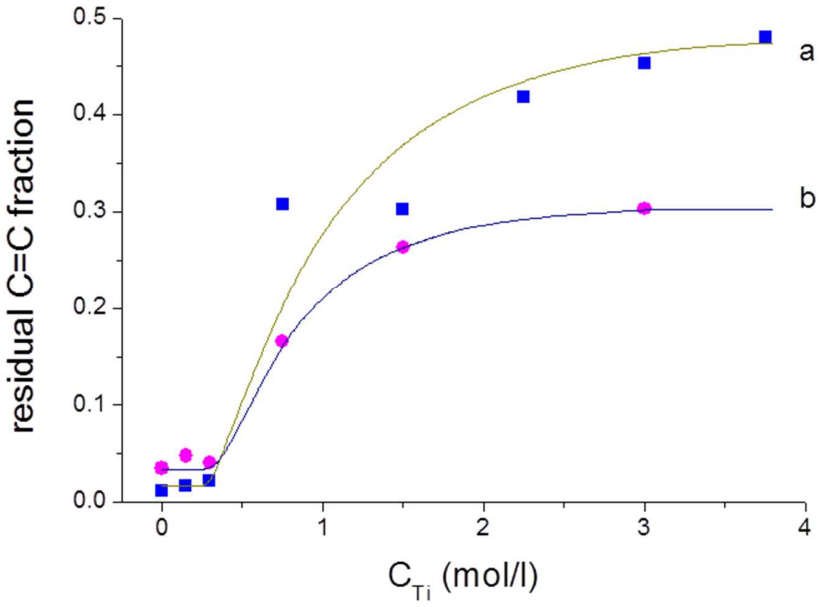

Figure 5. Residual monomer ratio after thermal polymerisation of HEMA-TiO_2 (a) and MAPTMS-TiO_2 (b) hybrids versus titania concentration (C_{Ti}).

Since TOA nanoparticles with similar size and concentration are used as the inorganic component of these hybrids, the difference was attributed to the organic-inorganic interface. The higher content of the non-polymerized monomers in HEMA compared to MAPTMS hybrids

supports our conclusion about the stronger bonding between its organic and inorganic components. Indeed, the monomers grafted onto the TOA nanoparticle surface possess much lower flexibility. Moreover, two types of sites can trigger polymerization: bulk monomers and those grafted on the TOA surface. This will reduce steric compatibility of the assembled chains and polymerization extent. In contrast, MAPTMS monomers not, grafted onto the TOA nanoparticle surface because of the silica shell, will conserve sufficiently high flexibility making the polymerization process more complete and its steric hindrance, due to the presence of the inorganic component, less pronounced.

An additional remark concerns mechanical quality of the HEMA and MAPTMS monolithic samples. While HEMA-TiO_2 samples were highly homogeneous and optically transparent, cracks appeared in bulk of the MAPTMS-TiO_2 samples after the preparation. The bulk stress due to the silica shell interlayer between the organic (MAPTMS) and inorganic (TiO_2) components seems to explain this fact.

3.2 Photonic sensitivity

The photonic sensitivity of the hybrids was obtained by the method explained in Refs[10,19]. The following major parameters were determined: the photo-induced charge separation efficiency (η) and the charge storage capacity (Q). The first one represents the initial slope of the darkening curve $\eta = \frac{dN_{Ti^{3+}}}{dN_{abs,photons}}$, while the second one represents the ratio between the charged photoinduced and total number of Ti centers in the unitary material volume: $Q = \frac{N_{Ti^{3+}}}{N_{Ti}}$.

The experimental dependences of the number of trapped electrons (per unit cross section) in the cell $N_{Ti^{3+}} = \int_0^L \left[Ti^{3+}\right](x)\,dx$ as a function of the UV laser irradiation doze are shown in Figure 6 for HEMA-TiO_2 and MAPTMS-TiO_2 hybrids with the titania concentration C_{Ti} = 1.5M. They

demonstrate better photosensitivity of the HEMA based hybrids compared to MAPTMS. Both the storage capacity and charge separation of the HEMA hybrids are significantly higher.

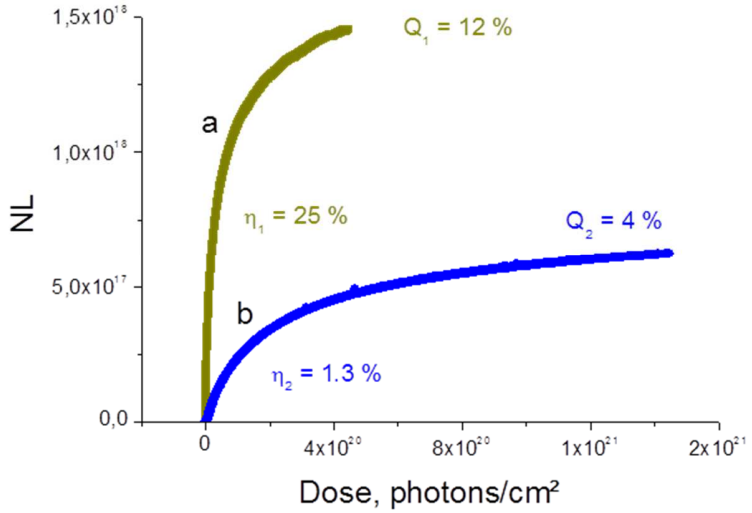

Figure 6. Photo-darkening kinetics of HEMA-TiO_2 (a) and MAPTMS-TiO_2 (b) hybrids X10 (excitation with 25 ps pulses of 5 mJ/cm^2 fluence at 355 nm), obtained after thermal organic polymerisation.

Comparison of the charge separation efficiencies in both hybrids as a function of Ti concentration is shown in Figure 7. In agreement with the proposed model of photo-induced processes in TiO_2 gels and hybrids[10], our present results evidence the efficiency of photoinduced charge separation in MAPTMS hybrids ~1.3 %, which does not significantly vary with the concentration of the inorganic component, TOA nanoparticles. Although no significant changes with the TOA nanoparticle concentration were found in HEMA hybrids, the charge separation efficiency was much higher, ~25 %. This strong difference can be assigned to the electronic coupling between the organic and inorganic components.

The charge separation process in nanoparticulate hybrid materials takes place at their large organic-inorganic interface. It is therefore reasonable to attribute the observed differences in the

charge separation efficiencies between HEMA-TiO_2 and MAPTMS-TiO_2 hybrids to the type of the interface.

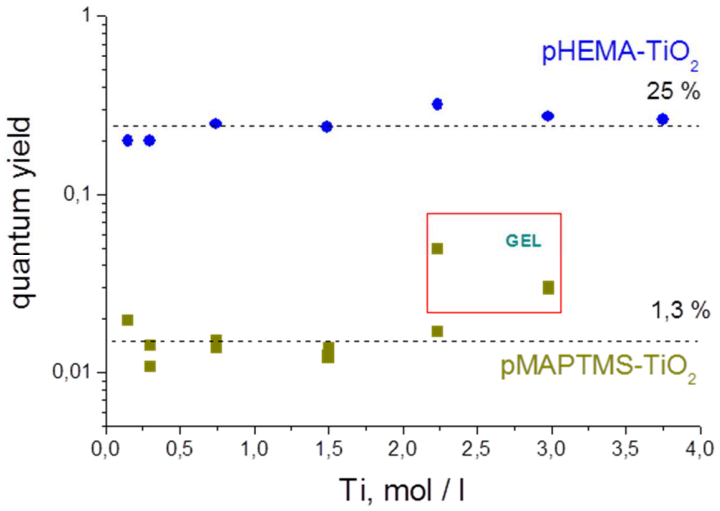

Figure 7. Charge separation efficiency in HEMA-TiO_2 and MAPTMS-TiO_2 hybrids (excitation with 25 ps pulses of 5-10 mJ/cm^2 fluence at 355 nm wavelength), obtained after thermal organic polymerisation.

According to Kuznetsov et al.[10], it is the hole that crosses the interface going from TiO_2 into the polymer component. Our present experiments show that HEMA-TiO_2 hybrids favor the hole exchange. Accordingly, the stronger bonds between titania and polymer domains produce better electronic coupling, which lowers the interface barrier between the valence band (VB) of TiO_2 and HOMO level of organics. Since VB of TiO_2 is formed by 3p(O) orbitals, the barrier height towards the hole exit depends on the electron affinity of the connected atoms in Ti-O-C and Ti-O-Si chains. The atomic electronegativities on Pauling scale are: χ(Ti)=1.54, χ(C)=2.55, χ(Si)=0.95 and the local charge on oxygen is expected to be higher when connected to Si/Ti then to Ti/Ti and C/Ti atoms. Consequently, the more localized 3p(O) orbitals in Ti-O-Si chains result in a higher potential barrier that slows down the hole transfer. Moreover, the surface silica layer

additionally isolates nanoparticle prohibiting the interface charge transfer in pMAPTMS-TiO_2 hybrids.

Several authors showed the detrimental effect of the silica shell. Guerrero-Martinez et al[35] showed the insulationg nature of silica by the influence of silica layer in the response of core shell under light irradiation for catalysis application. El Toni et al[36] showed also the decrease of the photocatalytic activity of TiO_2 by the presence of a layer of silica. Moreover, Viravathana et al[37] showed the impact of a layer of silica on titania with the objective of changing the refractive index. Our present results are in agreement with these observations.

3.3 Laser two-photon structuring

In order to test the ability of the synthesized hybrids for 2D/3D structuring, different microstructures have been fabricated using two-photon laser polymerization technique. This method consists in triggering radical organic polymerization in a small volume defined by the beam waist in the focal point. Two-photon polymerization was induced in liquid hybrid solutions, followed by the chemical developments in order to remove residual non-polymerized organic monomers.

Non-colored transparent structures of different shapes were obtained by this way from MAPTMS-TiO_2 hybrid solutions, see SEM images in Figure 8 (c) and (d).

Big box-like structures were produced using a laser beam loosely focused by 120 mm lens inside a thick flat layer of the hybrid solution. This kind of structures was used in order to check photochromic properties of the polymerized hybrids. In order to verify hybrids abilities for two-photon polymerization with micro- and nano-scale resolutions, woodpile-like structures have been fabricated. In this case, the laser beam was tightly focused using a 100× immersion oil microscope objective (Zeiss, Plan Apochromat, NA=1.4). These results demonstrate good

photoresist performance and the ability for fabrication of arbitrary structures targeted on desired applications.

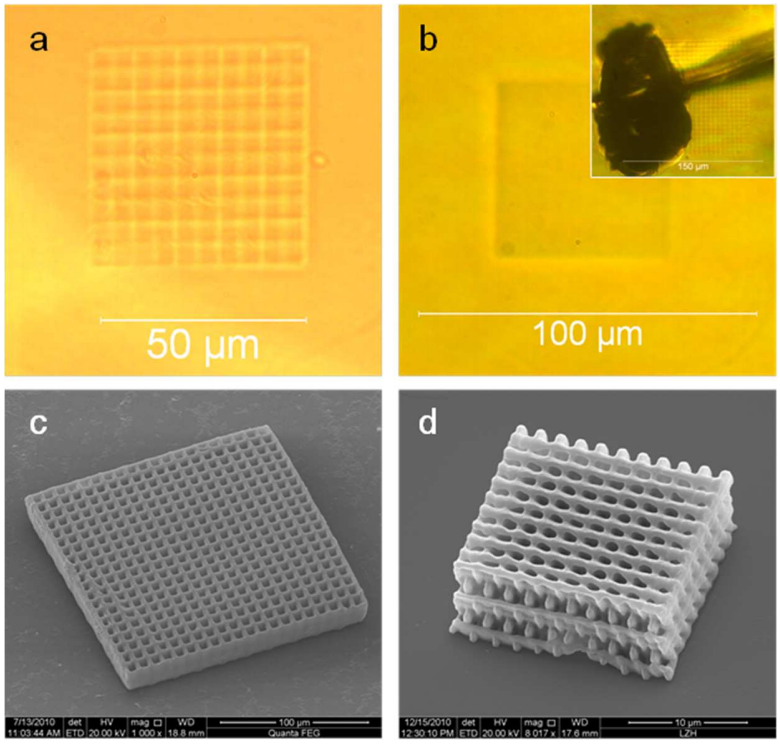

Figure 8. 2-photon laser structuring of HEMA-TiO_2 (a,b) and MAPTMS-TiO_2 (c,d) hybrids (femtosecond Ti-sapphire laser, 800 nm). The black cloud in inset of (b) shows a damage of the structure appeared during the writing process.

In contrast, we did not succeed in fabrication of stable stand-along solid hybrid structures from HEMA-TiO_2 solutions. In this case, shown in Figure 8 (a) and (b), we were capable fabricating toughness structures inside the hybrid solutions, which readily decompose at the development stage due to the ductility of the sample.

Attempts to reinforce these structures were unsuccessful, because even small fluctuations in the laser fluence exploded the structures as depicted in inset in Figure 8 (b). This structural

fragility of pHEMA-TiO_2 hybrids can be explained by their strong electron storage effectiveness[38]. We notice that at similar fluence conditions, MAPTMS-TiO_2 hybrid structures with higher mechanical properties were easily realized .

We notice that using one-photon polymerisation triggered by UV-visible lamps both HEMA-TiO_2 and MAPTMS-TiO_2 bulk solids were easily obtained. The obtained structures keep their photochromic properties inherent to the bulk hybrids.

4. Conclusion

The presented study is devoted to the comparison of structural organization and photonic sensitivities of two organic-inorganic hybrid materials based on TOA (TiO_2) nanoparticles included in different polymer phases, pHEMA and pMAPTMS.

We show that the TOA particle size and aggregation state are not affected by their concentration in HEMA solutions. In contrast, the TOA nanoparticles are bigger in MAPTMS environment and their concentration increase beyond 1.0 mol/l (Ti) results in aggregation. The ^{17}O NMR measurements indicate the preferential formation of Si-O-Si bonds compared to Ti-O-Si bonds in MAPTMS solutions. This is explained by the formation of a silica shell around the TOA nanoparticles prohibiting direct organic monomer grafting on the nanoparticle surface.

The monomer-to-polymer conversion in both hybrids with relatively small Ti concentration of $C_{Ti} \leq 0.75$ mol/l attains 100%. In contrast, the steric effect restricts the monomer conversion for higher Ti concentrations. The lower polymerization extent in HEMA-TiO_2 hybrids (compared to MAPTMS-TiO_2) is explained by lower flexibility of the grafted OEMA ligands, which serve to be a second center (after bulk monomers) for polymeric chains. On the other hand, stronger interaction between inorganic and organic components results in better mechanical stability of

the HEMA-TiO_2 hybrid solids.

The charge separation efficiency of 25% and long-term storage capacity of 12% were measured in HEMA-TiO_2 hybrids, while in MAPTMS-TiO_2 hybrids these values were considerably lower (1.3% and 4%, respectively) because of the presence of the silica shell.

3D solid structures were realized from MAPTMS-TiO_2 hybrid solutions by two-photon laser polymerization. At the same time, structuring of HEMA-TiO_2 hybrids was not successful and the produced structures were easily damaged during recording. This is explained by their high electron storage effectiveness leading to the material overheating and thermal explosion in course of the laser 2PP process. Moreover, because of the lower polymerization extent and insufficient cross-linking of the polymeric chains, fine HEMA-TiO_2 structures are fragile for the development. Consequently, from the practical point of view HEMA-TiO_2 hybrid shows better suitability for 2D/3D micropatterning related to photoinduced Ti^{4+}-Ti^{3+} reduction, whereas MAPTMS-TiO_2 hybrids are useful for 2D/3D micromachining, related to two-photon laser polymerization.

Acknowledgments. This work has been supported by I-20110047 EC project within EU contract ELISA-226716. The authors acknowledge the financial support of C'Nano IdF and IFR Paris-Nord Plaine of France. This scientific work has also been supported by the Grant RSF No. 16-13-10528 (for investigations of nanoparticle – organic interactions).

References

1. C. Sanchez, P. Belleville, M. Popall and L. Nicole, *Chem. Soc. Rev.* 40 (2011) 696-753.
2. L. Nicole, C. Laberty-Robert, L. Rozes and C. Sanchez, *Nanoscale* 6 (2014) 6267-6292.
3. G. Kickelbick, ed., *Hybrid materials, synthesis, characterization, and applications.*, Wiley-VCH, Verlag GmbH & Co. KGaA, 2007.
4. L. Nicole, L. Rozes and C. Sanchez, *Adv. Mater.* 22 (2010) 3208-3214.
5. C. Sanchez, L. Rozes, F. Ribot, C. Laberty-Robert, D. Grosso, C. Sassoye, C. Boissiere, L. Nicole, C. R. Chimie 13 (2010) 3.
6. A. Ovsianikov, A. Gaidukeviciute, B. N. Chichkov, M. Oubaha, B. D. MacCraith, I. Sakellari, A. Giakoumaki, D. Gray, M. Vamvakaki, M. Farsari, C. Fotakis, Laser Chemistry, 2008 (2008) 493059.
7. M. Farsari, M. Vamvakaki,B. N. Chichkov,J. Opt. 12 (2010) 124001.
8. I. Sakellari, A. Gaidukeviciute, A. Giakoumaki, D. Gray, C. Fotakis, M. Farsari, M. Vamvakaki, C. Reinhardt, A. Ovsianikov, B. N. Chichkov, Appl. Phys. A 100 (2010) 359.
9. O. Kameneva, A. Kuznetsov, L. A. Smirnova, L. Rozes, C. Sanchez, A. Alexandrov, N. Bityurin, K. Chhor, A. Kanaev, J. Mater. Chem. 15 (2005) 3380.
10. A. I. Kuznetsov, O. Kameneva, N. Bityurin,L. Rozes, C. Sanchez, A. Kanaev, Phys. Chem. Chem. Phys. 11 (2009) 1248-1257.
11. L. Museur, P. Gorbovyi, M. Traore, A. Kanaev, L. Rozes, C. Sanchez, J. Luminescence 132 (2012) 1192-1199.
12. E. Fadeeva, J. Koch, B. Chichkov, A. Kuznetsov, O. Kameneva, N. Bityurin, C. Sanchez, A. Kanaev, Appl. Phys A 84 (2006) 27.

13. A. Uklein, P. Gorboviy, M. Traore, L. Museur, A. Kanaev, Opt. Mater. Express 3 (2013) 533-545.
14. T. Cottineau, M. Richard-Plouet, A. Rouet, E. Puzenat, H. Sutrisno, Y. Piffard, P.-E. Petit, L. Brohan, Chem. Mater. 20 (2008) 1421.
15. T. Cottineau, L. Brohan, M. Pregelj, P. Cevc, M. Richard-Plouet, D. Arcon, Adv. Funct. Mater. 18 (2008) 2602.
16. N. Daude, C. Gout, C. Jouanin, Phys. Rev. B 15 (1977) 3229.
17. A. Henglein, Ber. Bunsenges. Phys. Chem., 86 (1982) 241.
18. A. Kuznetsov, O. Kameneva, A. Alexandrov, N. Bityurin, C. Sanchez, C. Chhor, Ph. Marteau, A. Kanaev, Phys. Rev. E 71 (2005) 021403.
19. P. Gorbovyi, A. Uklein, S. Tieng, M. Traore, K. Chhor, L. Museur, A. Kanaev, Nanoscale 3 (2011) 1807.
20. P. Gorbovyi, A. Uklein, M. Traore, L. Museur, A. Kanaev, Materials Research Express, 1 (2014) 045039.
21. E. Evlyukhin, L. Museur, A. P. Diaz-Gomez Trevino, M. Traore, O. Brinza, A. Zerr, A. Kanaev, Nanoscale 3 (2018) DOI: 10.1039/c8nr07868h
22. M. Rivallin, M. Benmami, A. Kanaev, A. Gaunand, Chem. Eng. Res. & Design 83(A1) (2005) 67.
23. R. Azouani, A. Michau, K. Hassouni, K. Chhor, J.-F. Bocquet, J.-L. Vignes, A. KanaevChem. Eng. Res. & Design, 88 (2010) 1123.
24. V. G. Kessler, J. Sol-Gel Sci. Technol. 51 (2009) 264.
25. R. Azouani, A. Soloviev, M. Benmami, K. Chhor, J.-F. Bocquet, A. Kanaev, J. Phys. Chem. C 111 (2007) 16243.

26. A. Kuznetsov, O. Kameneva L. Rozes, C. Sanchez, N. Bityurin, A. Kanaev, Chem. Phys. Letts. 429 (2006) 523.

27. J. Serbin, A. Ovsianikov, B. Chichkov, Opt. Express 12 (2004) 5221.

28. M. Farsari, B.N. Chichkov, Nature Photonics3 (2009) 450.

29. Y. Rao, T. F. Kemp, M. Trudeau, M. E. Smith, D. M. Antonelli, J. Am. Chem. Soc. 130 (2008) 15726-15731.

30. C. Gervais, F. Babonneau, M. E. Smith, J. Phys. Chem. B 105 (2001) 1971-1977.

31. P. Junlabhut, S. Booruang, W. Mekprasart, W. Pecharapa, Surf. Coat. Technol. 306 (2016) 262-266.

32. R. Sedghi, S. Asadi, B. Heidari, M. M. Heravi, Mater. Res. Bull. 92 (2017) 65-73.

33. S. Ali, Reference Module in Materials Science and Materials Engineering, 2018, Elsevier.

34. G. Mabilleau, C. Cincu, M. F. Basle, D. Chappard, J. Raman Spectr. 39 (2008) 767.

35. A. Guerrero-Martinez, J Perez-Juste, L. Liz-Marzan, Adv. Mater. 22 (2010) 1182-1195.

36. A. M. El-Toni, S. Yin, T. Sato, J. Colloid Interf. Sci. 300 (2006) 123-130.

37. P. Viravathana, D.W.M. Marr, J. Colloid Interf. Sci. 221 (2000) 301-307.

38. N. Bityurin, A. Kuznetsov, J. Appl. Phys. 93 (2003) 1567-1576.

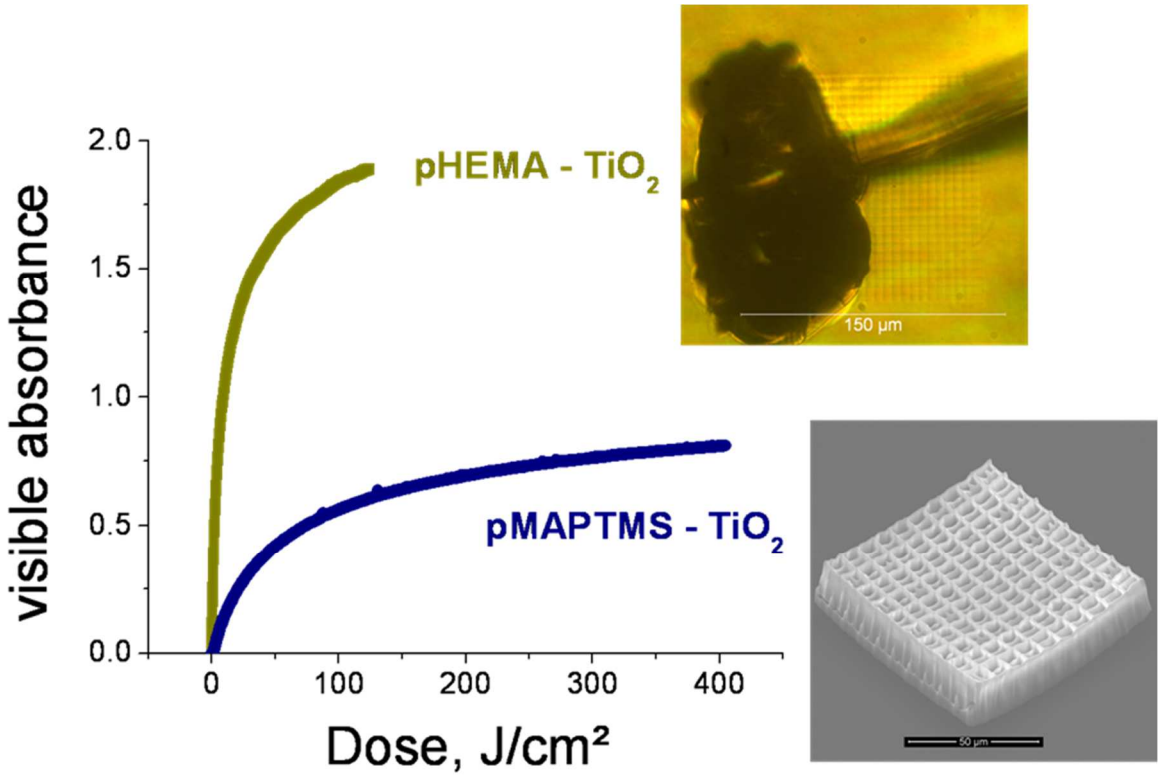

Photo-darkening kinetics (excitation with 25 ps pulsed of 5 mJ/cm^2 fluence at 355 nm) and 2-photon laser structuring (femtosecond Ti-sapphire, 800 nm) of HEMA-TiO_2 and MAPTMS-TiO_2 hybrids X10. The black cloud shows a damage of the structure appeared during the writing process in HEMA-TiO_2 hybrids.